

A New Rigid Connection for Heavy Beams and Columns in Steel Moment Resisting Frames

***Farzad Naeim, Kan Patel and Kai-Chen Tu
John A. Martin & Associates, Inc.
Los Angeles, California***

***M. "Saïd" Saïdi and Ahmad Itani
University of Nevada
Reno, Nevada***

***James C. Anderson
University of Southern California
Los Angeles, California***

Abstract

The 1994 Northridge earthquake revealed the vulnerabilities of the prevalent welded moment connections in Special Moment Resisting Frames (SMRF) at the time. Since then, extensive research has been performed to identify problems that caused poor performance of pre-Northridge welded moment connections and to come up with new moment connection solutions that can satisfactorily withstand the test of major earthquakes. Most of these efforts, however, are concentrated around connections consisting of beams and columns of small to moderate sizes. This paper presents a new SMRF connection suitable for tall buildings as well as projects that require long beam spans and tall story heights for their SMRF systems. The proposed connection has passed analytical as well as full-scale experimental studies with 20 in. and 24 in. square box columns and W36-W40 beams. A total of three laboratory tests were conducted and all specimens withstood large plastic rotation without any sign of deterioration in stiffness or strength.

Introduction

The 1994 Northridge earthquake revealed the vulnerabilities of the prevalent welded moment connections in Special Moment Resisting Frames (SMRF) at the time. Since then extensive research has been going on to identify the problems that caused poor performance of pre-Northridge welded moment connections and to come up with new moment connection solutions that can satisfactorily withstand the test of major earthquakes. Most of these efforts, however, are concentrated around connections consisting of beams and columns of small to moderate sizes (SAC, 1999).

Tall buildings as well as projects that require long beam spans and tall story heights for their SMRF systems generally require larger beams and column sizes for which test data may not be readily available. Although reduced beam section (RBS) is one of the most promising solutions to the SMRF problems, tests of RBS sections have demonstrated that once some plastification occurs at the reduced section, the beam web tend to buckle resulting in substantial reduction in strength and

stiffness of the beam and deterioration of the hysteretic characteristics. Although, this has not been a major problem with RBS connections since it has usually occurred after meeting the 3% plastic rotation required by current guidelines, the authors thought that postponing the beam web buckling may significantly enhance the performance of RBS connections.

The connection configuration presented in this paper (the JAMA connection) is a hybrid solution which is particularly suited for large, drift-sensitive, projects utilizing heavy beam and column sections. It utilizes a variety of concepts including bottom haunch, top cover plate, beam web stiffener, and reduced beam section (RBS). In this connection, the cross section of the beam is intentionally reduced within a segment to produce an intended plastic hinge zone. Contrary to conventional RBS solutions, the reduced section in JAMA connection is placed within the beam span away from the column face. The beam section between the reduced section and the face of the column is reinforced with a bottom haunch and a top cover plate in order to substantially reduce the seismic demand at the face of the column. The buckling of the web at the plastic hinge region is effectively postponed via the application of horizontal beam web stiffeners as shown in Figure 1.

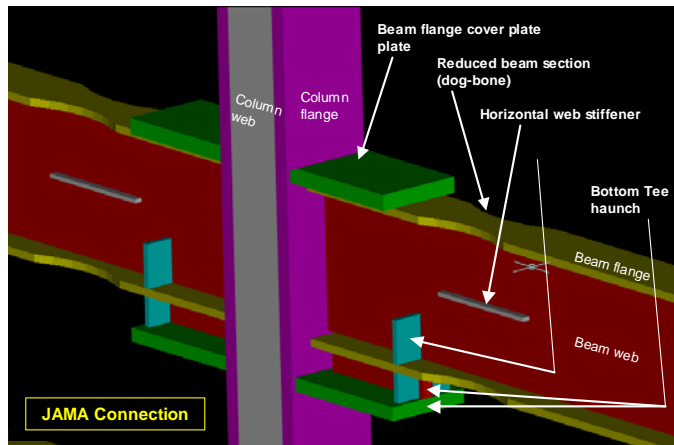


Figure 1. Illustration of the various components of a JAMA connection.

Analytical Validations

Detailed analytical validations of the proposed concept were performed using nonlinear finite element analysis techniques (see Figures 2 and 3) utilizing two independent computer programs namely COSMOS/M

(Naeim, 1999) and ADINA (Anderson, Xie and Naeim, 2001).

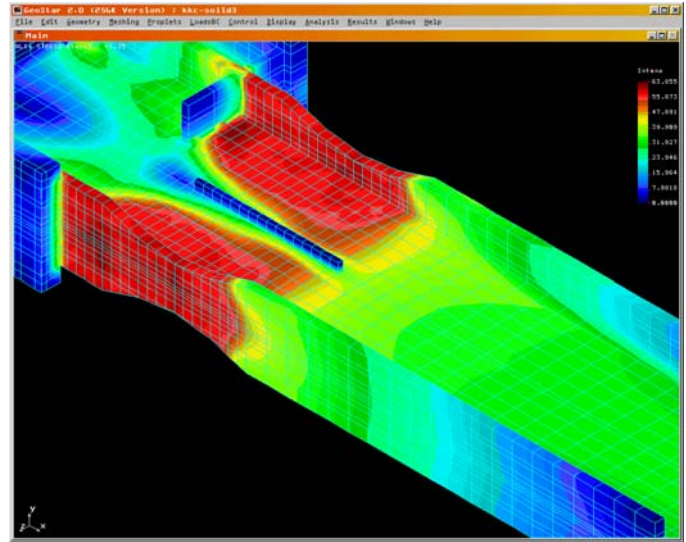


Figure 2. Von-Mises stress contours at full plastification of the RBS according to the pre-test finite element model (Naeim, 1999).

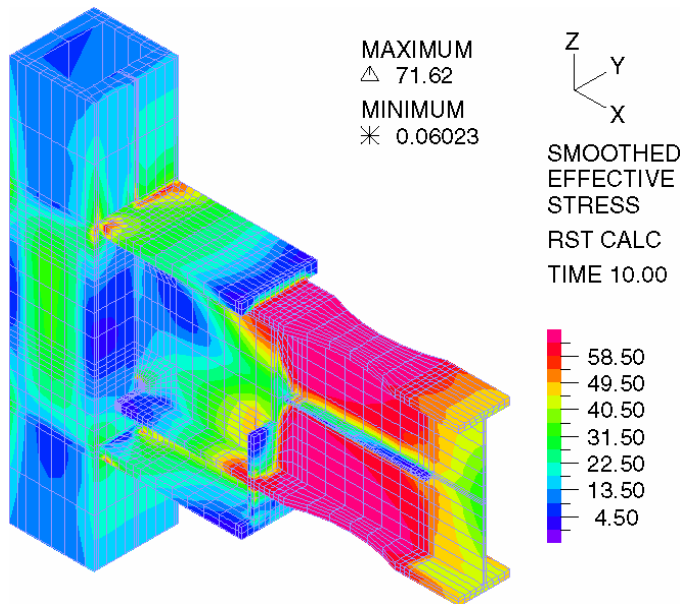


Figure 3. Smoothed Effective stresses at full plastification of the RBS according to one of the post-test finite element models (Anderson, Xie, and Naeim, 2001).

Both computer models used nonlinear solid elements but utilized different finite element meshing and nonlinear

solution scheme strategies. The results of both analyses confirmed the validity of the concept. The first set of analyses provided guidance for the refinement and adjustment of various components of the connection which were implemented before a set of full-scale cyclic tests were conducted at the University of Nevada, Reno. The second set of analyses were conducted following the experimental studies to further calibrate results of analysis with those observed from full-scale testing. Due to space limitations, in this paper we concentrate on the experimental results.

Details of Test Specimens

Three full-scale test specimens were tested under large cyclic deformations. The first specimen consisted of W36x232 beam and built-up box shape column 20"x20"x4"x2". The second and third specimens, identical specimens, consisted of W40x362 beam and built-up box shape column 24"x24"x4"x2". The first, second, and third specimens are designated as specimen 36-1, 40-1, and 40-2, respectively. A photo of the laboratory setup prior to testing is shown in Figure 4.



Figure 4. The laboratory setup for testing.

The RBS for specimen 36-1 started at a distance 41 in. from the face of the column. The beam flange width was reduced from 12.12 in. to 7.12 in. at the center of the RBS. Therefore, the percentage of the flange reduction is equal to 41%. The circular radius of the RBS was equal to 36 in. The cut edges of the beam were grounded in the direction of the flange length. The

surface roughness was specified to meet the requirements of AWS C4.1-77 Class 4. All corners were rounded to minimize any notch effects. A horizontal web stiffener 1"x2"x3'-0" was added at web mid-height at each side of the web to delay web local buckling. More details of a typical test specimen are shown in Figures 5 to 9, respectively.



Figure 5. The 36-1 specimen in place ready for testing. The areas of concern are whitewashed to show possible signs of distress.



Figure 6. The two actuators used in series to force cyclic displacement at the end of the beam.

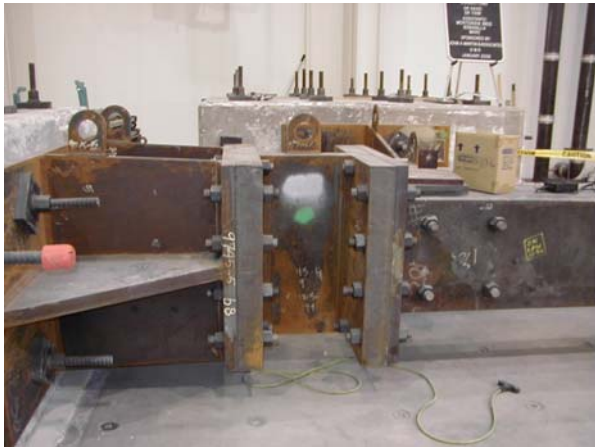


Figure 7. The column ends are restrained by attachments to the resistance block.



Figure 8. The control computer and electronics.



Figure 9. Whitewashed and instrumented bottom RBS and haunch.

For the 36-1 specimen the compactness ratio of the beam at the RBS was equal to 2.27. This value is almost one third of the specified limiting width-thickness ratio of the AISC Seismic Provisions. This would suggest that the flanges are “extra” compact sections and may not exhibit plastic local buckling under large strains. The horizontal web stiffener reduced the web compactness ratio by $\frac{1}{2}$. The compactness ratio of the web is equal to 18.7, which is almost one third of the specified limiting width-thickness ratio of the AISC Seismic Provisions (AISC, 1997).

The RBS for specimen 40-1 and 40-2 started at a distance 43 in. from the face of the column. The beam flange width was reduced from 16 in. to 9 in. at the center of the RBS. Therefore, the percentage of the flange reduction is equal to 44%. The circular radius of the RBS was equal to 36 in. The cut edges of the beam were grounded in the direction of the flange length. The surface roughness was specified to meet the requirements of AWS C4.1-77 Class 4. All corners were rounded to minimize any notch effects. A horizontal web stiffener 1”x2”x3’-0” was added at web mid-height at each side of the web to delay web local buckling.

The compactness ratio of these beams at the RBS was equal to 2.25. This value is almost one third of the specified limiting width-thickness ratio of the AISC Seismic Provisions. This would suggest that the flanges are “extra” compact sections and may not exhibit plastic local buckling under large strains. The horizontal web stiffener reduced the web compactness ratio by $\frac{1}{2}$. The compactness ratio of the web is equal to 15.3, which is slightly more than one fourth of the specified limiting width-thickness ratio of the AISC Seismic Provisions.

The test specimens were fabricated at Herrick, Stockton, CA and were delivered to UNR Structural Laboratory. All beam-to-column welding were performed at UNR lab with the columns up right position to simulate the actual field conditions. The welding was performed according to the Welding Procedure Specifications (WPS) and was continuously monitored by a certified welding inspector. The specified welding electrodes were of low hydrogen and have a minimum charpy V-Notch toughness of 20 ft-lb at -20° F.

The material for the specimens met the requirements of ASTM A6 with a CVN of 20 ft-lb at 70° F. Coupon tests

were conducted at Consolidated Engineering Laboratory, Oakland, CA. The yield stress and ultimate strength of specimen 36-1 were equal to 61 ksi and 73, respectively. The yield stress and ultimate strength were equal to 50.9 ksi and 71 ksi for 40-1 and 40-2 specimens, respectively.

Test Set-up and Instrumentation

The actuators were attached to three 8 ft. x 4 ft. x 4ft. reaction blocks and to the actuator guide as shown in Figure 4. The guide was attached to the beam through a 3½ in. diameter pin. The column was attached to two brackets as shown in Figure 3 to resist the axial force and the shear applied at its supports. Bracket A was attached to two reaction blocks while bracket C was attached to three reaction blocks.

The lateral actuators, MTS model 243.80 and 243.90, were under displacement control. The two actuators combined were able to apply 650 kips and ± 9 in of movement in each direction. No lateral bracing of beam flanges were provided except at the actuator location. The Inspector of Record monitored all the tests, while OSHPD representatives witnessed the second and the third tests.

Fifty strain gauges YFLA-5-5L, manufactured by Tokyo Sokki Kenkyujo Co., Ltd., Japan were used on several locations of the beam and the column to measure the strain. According to the manufacturer, these strain gauges are post yield gauges capable of reading strain up to 10%. Three YFRA 45/90 3-element rosettes were mounted on the beam and the column panel zone. Six cable extension transducers were used to measure the displacement at the tip of the specimen, middle of the RBS, at the column panel zone, and behind the column. The transducers were Novotechnick TR-50 type with a resolution of 0.0004 in. All the measuring devices were connected to Megedec 310DC data acquisition system, which was set at a sample rate of one reading per second. Details of test conditions and results will be available shortly in a University of Nevada, Reno report (Saiidi, Itani, and Naeim, 2000).

Loading History

The test specimens were subjected to cyclic loads according to an OSHPD approved testing protocol which was similar to AISC Seismic Provisions. The

specimens were considered to satisfy acceptance requirements if they sustained two cycles of deformation at or above 3% plastic rotation measured from the center of the plastic hinge zone with no significant reduction in hysteretic characteristics. The tests were conducted by controlling the level of deformation imposed on the specimens. The value of significant yield displacement (δ_y) was determined based on the strain gauge readings at the RBS. The yield displacements were equal to 1.5 and 1.3 inches for specimens 36-1 and 40-1/2, respectively. Loads were applied to the test specimens to produce the following deformations:

- 3 cycles of loading at: $0.5\delta_y$
- 3 cycles of loading at: $0.75\delta_y$
- 3 cycles of loading at: δ_y
- 3 cycles of loading at: $2\delta_y$
- 3 cycles of loading at: $3\delta_y$
- 2 cycles of loading at: $4\delta_y$

After completion of the loading cycles at $4\delta_y$, testing was continued by applying cyclic loads to produce $5\delta_y$, $6\delta_y$, $7\delta_y$, etc. Two cycles of loading were applied at each of these subsequent deformation values.

Experimental Performance of Test Specimens

Test Specimen 36-1

Photos taken from various stages of testing of this specimen are presented in Figures 10 to 16. The force-displacement characteristics of specimen 36-1 are shown in Figure 17 where the horizontal axis represents the lateral displacement applied at the pin and the vertical axis represents the shear applied by the two actuators. Initial yielding occurred during cycles 7 and 8 at $\delta_y=1.5$ inches. The yielding was observed at RBS of both flanges. Progressing through the loading history, yielding started to propagate along the RBS. During cycle at $4\delta_y$ (4.1% plastic rotation) initiation of web buckling was noted on both sides of the top and bottom flanges. With the increasing of the displacement the web started to experience serve local buckling and initiation of plastic local buckling in the flanges. The web buckling and the significant yielding of the flanges limited the capacity of the beam. It should be noted here

that the web buckling was not accompanied with any drop in the load capacity of the assembly.

During the second cycle at $6\delta_y$ (6.8% plastic rotation) a crack was developed in the middle of RBS bottom flange. Upon progressing through the loading history, the crack spread rapidly across the bottom flange and propagated through the web. Due this fracture the lateral load capacity started to deteriorate as can be seen in the hysteresis loops. The test was stopped because of the severe deformation of the specimen and the significant drop in the lateral capacity. The maximum force that the specimen was subjected to was 378 kips.

There were no signs of yielding in the column. The column panel zone stayed in the elastic range as the white wash stayed intact. The readings of the 45/90 rosette, mounted in the middle of the column panel zone, is shown in Figure 18. As can be seen from this figure, the strains were well below the yield strain indicating that the column web zone stayed in the elastic range. The maximum ratio of the shear deformation to the total deformation was 3.3%. Therefore, contribution of panel zone distortion to the deformation of the assembly was negligible and the panel zone could be assumed fully rigid for design calculations. This fact was further confirmed by post-testing nonlinear finite element analyses (Anderson, Xie, and Naeim, 2001).

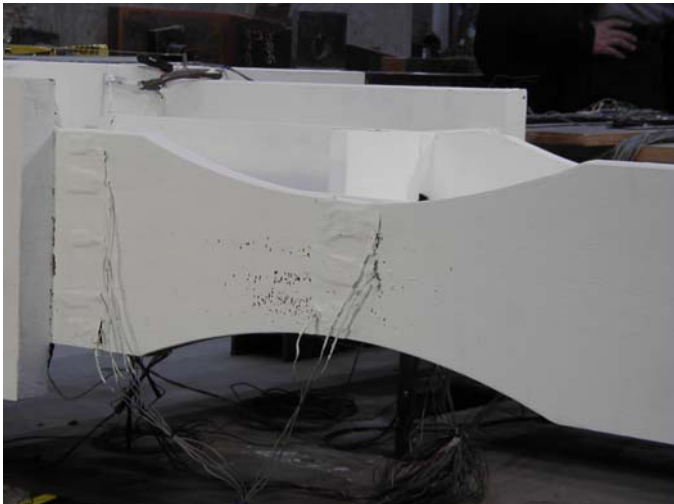


Figure 10. The onset of yielding of Specimen 36-1 at $\delta = \delta_y = 1.5$ in.



Figure 11. As predicted by our nonlinear finite element analysis (Naeim, 1999), at low amplitude cycles there would be some rise in stress along the tip of the cover plate that would subside as the specimen would go into nonlinear range. That is exactly what happened. This picture is taken at yield displacement.

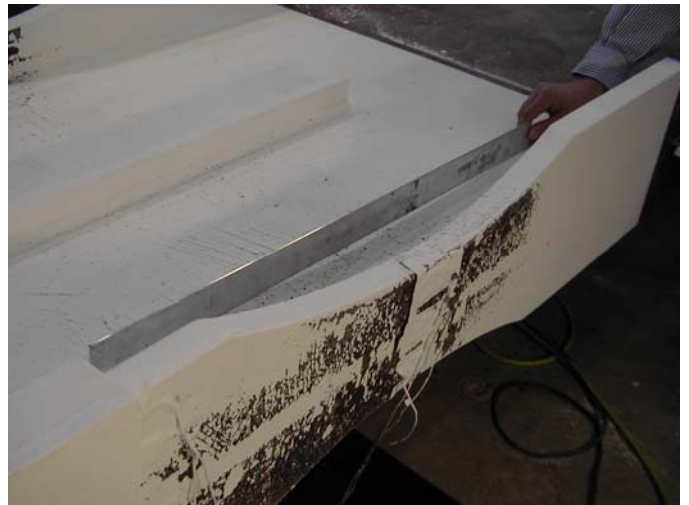


Figure 12. Specimen 36-1 at displacement of $2\delta_y$. Yielding of RBS flange is extended and signs of web buckling above the web stiffener may be seen.



Figure 13. At the end of $3\delta_y$ cycles or 2.7% plastic rotation web buckling may be observed, but no strength reduction is yet noticed (photo of specimen 36-1).



Figure 14. At $3\delta_y$ a crack at the tip of the beam flange at the termination of cover plate was observed in all three specimens. This crack however did not grow in size or length during the remaining cycles of the test and did not adversely affect the hysteretic characteristics.



Figure 15. At the end of regulatory testing or 4% plastic (6.8% total) the specimen (36-1 showed here) is still showing increasing capacity and no loss of stiffness is present. Plastification of RBS flanges, buckling of the beam web and some local buckling of the RBS flange may be observed.



Figure 16. Finally, at $5\delta_y$ (5.4% plastic rotation, 6.8% total rotation) failure of 36-1 specimen starts by tension failure of the bottom flange at the center of RBS and propagates into the web. Specimens 40-1 and 40-2 stayed course as the actuators ran out of stroke at plastic rotations exceeding 7%.

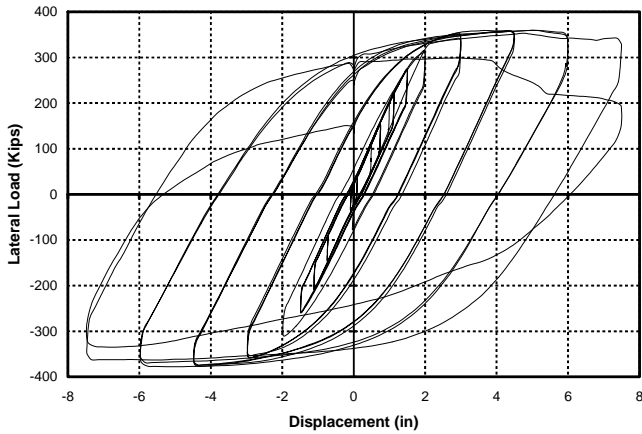


Figure 17. Force-displacement response of specimen 36-1.

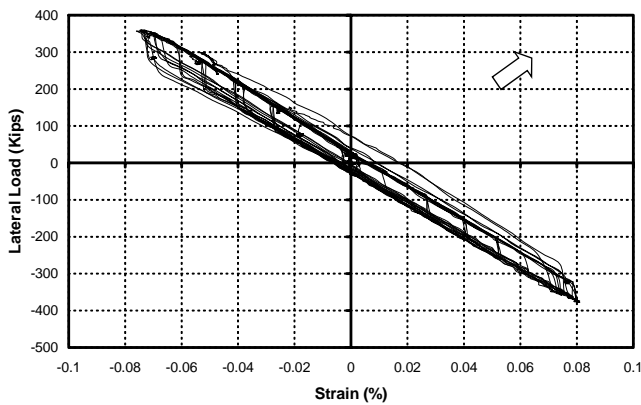


Figure 18. Strain data of panel zone rosette of specimen 36-1.

Test Specimens 40-1 and 40-2

Specimens 40-1 and 40-2 were identical specimen and showed similar behavior during the cyclic testing. The response of specimen 40-2 is shown in Figure 19. Initial yielding occurred during cycles 7 and 8 at $\delta_y=1.3$ inches. Progressing through the loading history, the yielding started to spread across the RBS at both top and bottom flange. The process of plastification was characterized by propagation of the yield pattern along the beam flanges and by yielding of the beam web. The energy dissipated is reflected by wider hysteretic loops. The ultimate resisting force of the specimen was 620 kips. During the 4 δ_y cycle (3.6% plastic rotation) plastic local buckling started to occur in the web. This local buckling did not cause any deterioration of the load capacity as can be seen in the hysteresis plot.

At this stage of the test, the regions in the specimen away from the plastic zone were carefully inspected for signs of yielding and damage. Several local yield lines were observed in a region adjacent to the RBS, however yielding was not observed adjacent to the beam-column connection. Increasing the deformation demand was accompanied by a minor plastic local buckling in the flange RBS zone. Two cycles of displacement at $7 \delta_y$ corresponding to the maximum stroke of the actuators did not cause failure in specimen 40-1 and the test was stopped at that point. The same results were obtained for specimen 40-2. This time, however, the cycles were repeated till failure of the specimen occurred by local buckling of the flange at the reduced section which finally led to a crack. The flange then started to tear across its thickness and propagating through the flange causing a drop in the lateral capacity.

There were no signs of yielding in the column. The column panel zone stayed in the elastic range as the white wash stayed intact. The readings of the 45/90 rosette, mounted in the middle of the column panel zone, are shown in Figure 20. As can be seen from this figure, the strains were well below the yield strain indicating that the column web zone stayed in the elastic range. The maximum contribution of shear deformation to total deformation was about 3.4%.

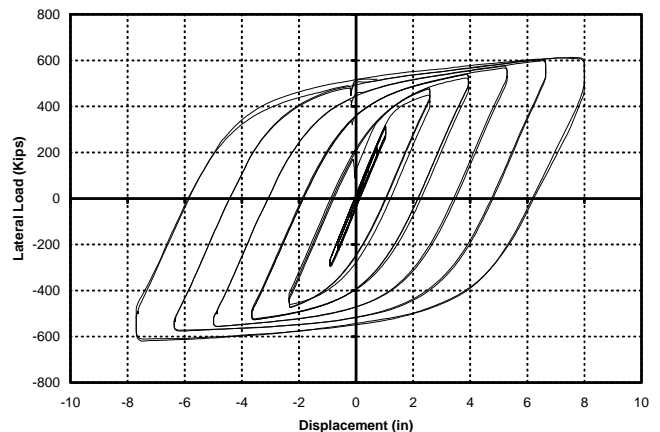


Figure 19. Force-displacement response of specimens 40-1 and 40-2.

Moment-Rotation Relations Measured from the Center of plastic hinge

The total-moment rotation plots for the specimens are presented in Figures 21 and 23. The moment in these

plots is defined as the shear force as applied by the actuators multiplied by the centerline distance of the pin from the middle of the RBS. The rotation is defined as the lateral displacement at the pin divided by the centerline distance of the pin from the middle of the RBS. The value of the rotation defined in this way includes contribution from both elastic and inelastic deformation. A response of greater interest than the total rotation is the plastic rotation, θ_p . The plastic rotation was computed for the specimens as follows

$$\theta_p = \theta - \frac{V}{K_e}$$

where V is the shear force and K_e is the ratio of V/θ in the elastic range. Figures 22 and 24 show the moment versus the plastic rotation of specimens 36-1 and 40-1/2.

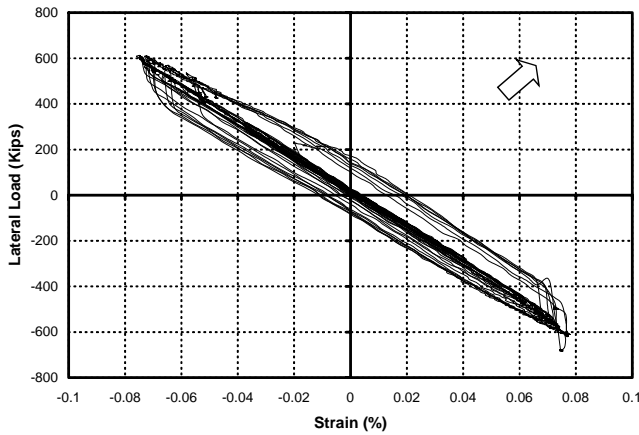


Figure 20. Strain data of panel zone rosette of specimen 40-2.

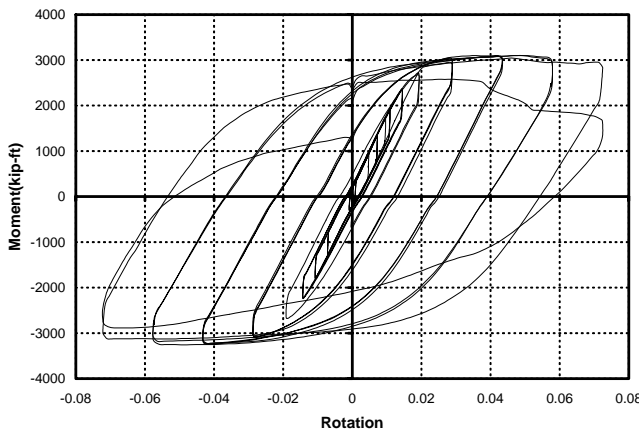


Figure 21. Moment-rotation response of specimen 36-1.

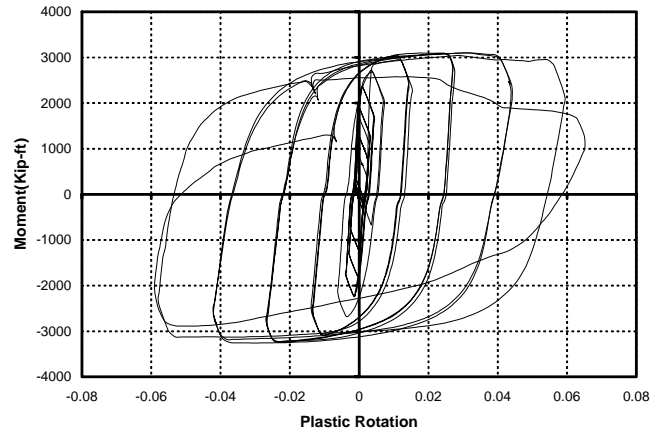


Figure 22. Moment-plastic rotation response of specimen 36-1.

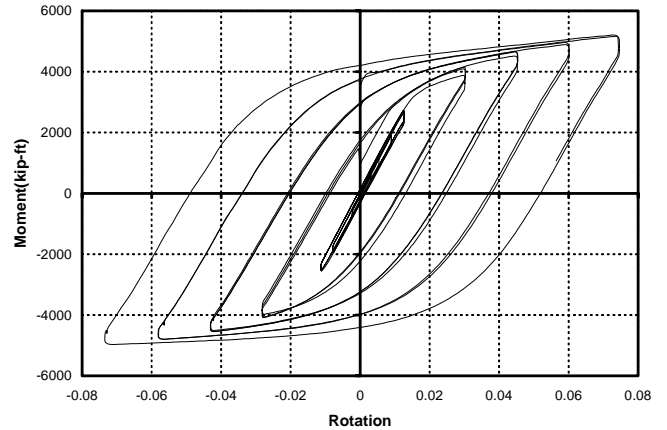


Figure 23. Moment-rotation response of specimens 40-1 and 40-2.

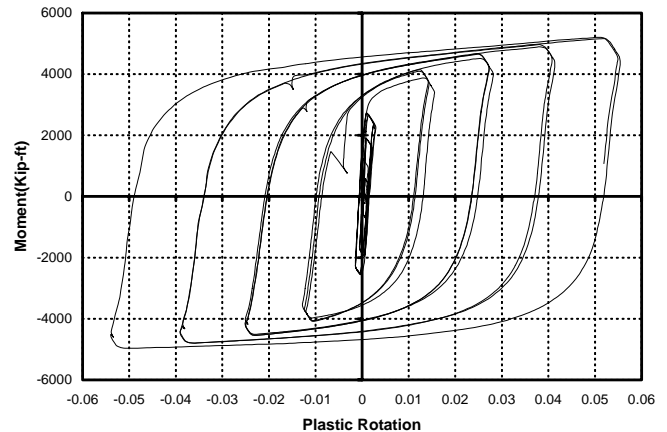


Figure 24. Moment-plastic rotation response of specimens 40-1 and 40-2.

As can be seen from these figures, specimen 36-1 reached almost 6% radians of plastic rotation, while specimen 40-2 exceeded 5% radians of plastic rotation.

Moment-Rotation Relations Measured from the Center-line of the Column

Obviously, plastic rotations will be smaller if measured from the centerline of the column rather than the center of RBS. Formula 7-1 of the FEMA-267 imposes a plastic rotation demand of 0.03 radians. If, however, center-to-center spacing of columns (L) is more than 1.25 times the center-to-center spacing of the plastic hinges (L'), then the plastic rotation demand is calculated from the formula:

$$\theta = 0.025 \left[1 + \frac{(L-L')}{L'} \right]$$

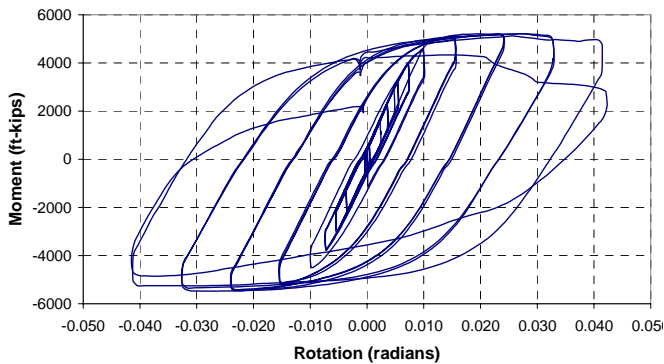


Figure 25. Moment-plastic rotation response of specimen 36-1 (rotation measured from the centerline of the column).

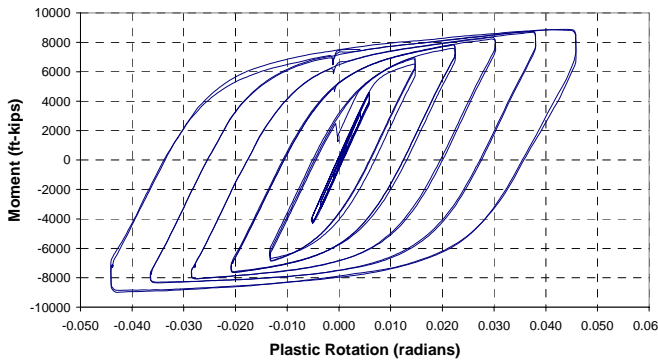


Figure 26. Moment-plastic rotation response of specimens 40-1 and 40-2 (rotation measured from the centerline of the column).

The moment-plastic rotation responses of the smaller and larger specimens as measured from the centerline of the column are presented in Figures 25 and 26, respectively. Calculations showing that the tested specimens passed this requirement are summarized below:

FEMA-267 Plastic Rotation Demands

- W36: $\theta = 0.025 \left[1 + \frac{(L-L')}{L'} \right] = 0.025 \left[1 + \frac{(174.00-109.75)}{109.75} \right] = 0.0396$
- W40: $\theta = 0.025 \left[1 + \frac{(L-L')}{L'} \right] = 0.025 \left[1 + \frac{(174.00-103.50)}{103.50} \right] = 0.0420$

Observed Plastic Rotation Capacities

- W36: $\theta = \frac{(\delta_{total} - \delta_y)}{\left(\frac{L}{2}\right)} = \frac{[6(1.5) - 1.5]}{(174.0)} = 0.0431 > 0.0396$
- W40: $\theta > \frac{(\delta_{total} - \delta_y)}{\left(\frac{L}{2}\right)} = \frac{[9.25 - 1.10]}{(174.0)} = 0.0474 > 0.0420$

Conclusion

A new rigid SMRF connection configuration suitable for application in tall buildings as well as other large drift sensitive structures was presented. This connection which showed promise during analytical investigations was subjected to three full-scale tests using box columns and heavy W36 and W40 beam sections. All three test specimens performed exceptionally well. They all comfortably exceeded the required 3% plastic rotation without deterioration. The specimens showed very reliable performance during the cyclic test under the demanding loading history. The plastic hinged formed inside the RBS as intended and did not spread to the beam-column connection. The specimens maintained high strength as well as high ductility during the cyclic tests. The beam-column panel zones stayed rigid during the course of these experiments. Therefore, the assumption of 100% rigidity of panel zone for structural analysis and design purposes was verified. Furthermore, the damaged specimens showed a stable behavior without any sudden loss of stiffness. It is hoped that this new contribution to the possible SMRF solutions will find widespread acceptance and use by structural engineers responsible for designing major structures in seismic regions.

References

American Institute of Steel Construction, (1997), *Seismic Provisions for Structural Steel Buildings*, Chicago, Illinois.

Anderson J. C., Xie, L., and Naeim, F., 2001, *Nonlinear Finite Element Analysis of JAMA SMRF Connection*, University of Southern California, Los Angeles.

FEMA-267, 1995, *Interim Guidelines, Inspection, Evaluation, Repair, Upgrade and Design of Welded Moment Resisting Steel Structures*, Prepared by SAC Joint Venture.

FEMA-350, 2000, *Recommended Seismic Design Criteria for New Steel Moment-Frame Buildings*, Prepared by SAC Joint Venture.

Naeim, F., 1999, *Nonlinear Finite Element Analysis Verification of JAMA-KKC Connection Concept*, Internal Report, John A. Martin & Associates, Inc., Los Angeles.